EPJ E
Soft Matter and Biological Physics
EPJ.org
your physics journal

Eur. Phys. J. E (2013) **36**: 124 DOI 10.1140/epje/i2013-13124-x

# Electro-hydrodynamic instability of stressed viscoelastic polymer films

F. Closa, E. Raphaël and F. Ziebert

edp sciences Società Italiana di Fisica Springer

Eur. Phys. J. E (2013) **36**: 124
DOI 10.1140/epje/i2013-13124-x

THE EUROPEAN PHYSICAL JOURNAL E

Regular Article

# Electro-hydrodynamic instability of stressed viscoelastic polymer films

F. Closa[1], E. Raphaël[2], and F. Ziebert[3,4,a]

[1] Laboratoire de Physique Théorique de la Matière Condensée - UMR 7600 LPTMC, Université Pierre et Marie Curie Paris 6, 4 place Jussieu, 75252 Paris, France
[2] Laboratoire de Physico-Chimie Théorique - UMR CNRS Gulliver 7083, ESPCI, 10 rue Vauquelin, 75231 Paris, France
[3] Physikalisches Institut, Albert-Ludwigs-Universität, 79104 Freiburg, Germany
[4] Institut Charles Sadron, 23 rue du Loess, 67034 Strasbourg, France

Received 2 August 2013
Published online: 28 October 2013 – 

**Abstract.** We study the stability of a viscoelastic thin polymer film under two destabilization factors: the application of an electric field normal to the surface —as in typical electro-hydrodynamic destabilization experiments— and the presence of a frozen-in internal residual stress, stemming from the preparation process of the film, typically spin-coating. At the film-substrate interface we consider a general boundary condition, containing perfect gliding on slippery substrates, as well as perfect sticking of the film to the substrate as limiting cases. We show that the interplay of the two sources of stress, the viscoelasticity and the boundary condition, leads to a rich behavior, especially as far as the fastest growing wave number (or wavelength) is concerned. The latter determines the initial growth of the instability, and often also the final pattern obtained in small capacitor gaps, and is the main experimental observable.

## 1 Introduction

Thin films containing polymers are ubiquitous in technological applications. On the one hand, their stability and how the film geometry as well as the production process interfere with it, is an important issue. On the other hand, detailed studies of the destabilization of such films [1,2] shed new light on the behavior of polymers and on their conformations that differ from those in the bulk due to the confinement in the thin film and the out-of-equilibrium production process.

Spin coating is probably the most popular coating technique for polymer films [3,4]. Starting from a dilute polymer solution, the rapid solvent evaporation during the spinning leads to frozen-in residual stresses in the film that finally turns glassy. These stresses are tensile and can be up to 100 MPa, comparable to the film's elastic modulus; they have been evidenced by various experiments, among others by dewetting studies [5,6] and by electro-hydrodynamic destabilization, where the film is coated on one of the plates of a capacitor [7]. In these experiments the films are liquefied by heating them up beyond the glass transition temperature, $T_g$. Other methods, that can deal also with glassy films, are surface wrinkling [8], where the thin film is coated on an elastomeric substrate under tension, as well as micro-cantilever experiments [9]. The frozen-in stresses have to be found to relax very slowly, and recent dewetting experiments [10] supported by modeling [11,12], could relate this relaxation to segmental relaxations.

For as-cast as well as aged thin films of polystyrene, the electro-hydrodynamic instability (EHI) [13] was recently investigated in much detail [7]. By means of a laser interferometric method, both the fastest growing wave numbers and the growth rates of the resulting surface undulations could be studied as a function of sample age, *i.e.* stress. Although the EHI geometry is better defined than the dewetting geometry, theoretically the problem is not yet well understood, because there are two acting stresses that interplay —the in-plane residual stress and the electric stress normal to the surface. In addition, the system is sensitive to viscoelastic effects and, in general, to the boundary condition at the substrate. While in the absence of stress, numerous theoretical studies of EHI exist for the elastic [14], viscoelastic [15] and liquid case [16], the effect of residual stress has been started to be investigated only recently [17,18].

Here we study a thin polymer film —described by a Maxwell viscoelastic fluid and containing a frozen-in residual stress— in the electro-hydrodynamic destabilization geometry. As suggested by experiments [19,7], the residual stress is assumed not to relax on the time scale of the growth of the linear instability. The film is considered to be purely dielectric, which is more suitable for a polystyrene melt than the "leaky dielectric" case [20], often considered

[a] e-mail: fziebert@gmail.com

in EHI [21,16]. To be as general as possible, we accounted for a boundary condition ("imperfect gliding") at the film-substrate interface, that contains both slippery and sticky substrates as limiting cases. Within this modeling framework, we study how the surface instability is influenced by the combined action of both stresses, the viscoelasticity and the boundary conditions.

The work is organized as follows: in sect. 2 we discuss the modeling framework, using nonlinear elasticity to implement the residual stress and the Maxwell model to implement the liquification of the stressed film upon heating up above the glass transition temperature. We also discuss the boundary conditions. In sect. 3, we give some information about how the linear stability analysis is performed. Details can be found in appendix A. In sect. 4 we discuss all relevant parameters. In the main sect. 5 we show and discuss our results and we conclude in sect. 6.

## 2 Model framework

We consider the typical geometry of the electro-hydrodynamic instability (EHI): a polymer film is spin-cast on one of the plates of a capacitor. The distance between the two plates is given by $d$, the film thickness is $h_0$. The gap between the film and the opposite plate, $d - h_0$, is filled with air. The film is initially flat, hence the electric field is initially normal to the film when a voltage is applied. Assuming a perfectly dielectric polymer film, the arising electric Maxwell stress then will favor the film's surface to be parallel to the field lines [22], giving rise to the EHI.

The polymer film is modeled as a viscoelastic Maxwell fluid, *i.e.* by a constitutive law that describes elastic behavior at short times, $t < \tau_M$, and viscous behavior at long times, $t > \tau_M$. The characteristic time scale $\tau_M$ is given by the ratio of the viscosity $\eta$ and the elastic shear modulus $G$. The Maxwell model (and generalizations thereof) corresponds best to the experimental situation where the film is heated up from a temperature below the glass transition temperature —where the film is elastic— to a temperature above where the film liquefies, as discussed in sect. 2.2. At first, we have to give some details on the nonlinear elasticity formulation [17], applied to properly include the residual stress.

### 2.1 Nonlinear elasticity and residual stress

As spin-coating is a complex process and its consequences on the conformations and properties of polymer films are still under debate [4], we chose a simple "preparation protocol" [17], giving rise to in-plane stresses in the film.

Assume that at first the film is in a stress-free state given by the coordinates $\mathbf{X} = X_i \mathbf{e_i}$. Then the film is stretched (or compressed) uniaxially in the $x$-direction by a stretch factor $\lambda > 1$ (or $\lambda < 1$, respectively). This new state has coordinates $\mathbf{x} = x_i \mathbf{e_i}$ and will be called the *base state*. It experiences a uniaxial stress $\sigma^0_{xx}$, cf. below. Finally, the film is brought in perfect contact with the substrate, imposing the boundary conditions discussed in sect. 2.3. If heated above $T_g$, the film will evolve —under the in-plane stress and the normal electric stress— yielding the *current state*, described by coordinates $\tilde{\mathbf{x}} = \tilde{x}_i \mathbf{e_i}$. For simplicity, and as a good approximation for elastomers and polymer melts, the film is considered to be incompressible.

The total deformation gradient tensor, relating the coordinates $\mathbf{X}$ to the ones $\tilde{\mathbf{x}}$ in the current state, can be expressed as

$$\boldsymbol{F} = \frac{\partial \tilde{\mathbf{x}}}{\partial \mathbf{X}} = \frac{\partial \tilde{\mathbf{x}}}{\partial \mathbf{x}} \cdot \frac{\partial \mathbf{x}}{\partial \mathbf{X}} =: \boldsymbol{F}_2 \cdot \boldsymbol{F}_1 \,. \tag{1}$$

Here $\boldsymbol{F}_1 = \mathrm{Diag}(\lambda, \lambda^{-1/2}, \lambda^{-1/2})$ describes the stretch/compression of the film (Diag being the $3 \times 3$ diagonal matrix). Since we consider finite stresses, it is this step that requires the nonlinear formulation. For the second tensor, a linear description is sufficient, and by introducing $\tilde{\mathbf{x}} = \mathbf{x} + \mathbf{u}$, it is given by $\boldsymbol{F}_2 = \boldsymbol{I} + \nabla \mathbf{u}$. Here $\boldsymbol{I}$ is the identity tensor and $\nabla \mathbf{u} = (\partial_j u_i)_{ij}$ is the displacement gradient tensor known from linear elasticity theory. It describes displacements in the current state with respect to the stretched state, and is hence the quantity to study the evolution of the stretched base state.

In nonlinear elasticity, the tensor describing the stress after a deformation in the current configuration per unit area of the current configuration is the so-called Cauchy stress tensor. Introducing the left Cauchy-Green tensor, $\boldsymbol{B} = \boldsymbol{F} \cdot \boldsymbol{F}^{\mathrm{T}}$, it is defined as

$$\boldsymbol{\sigma}^{\mathrm{NH}} = G\boldsymbol{B} - p\boldsymbol{I} \,, \tag{2}$$

where we used a Neo-Hookean elastic solid [23], which is also the limit of the Maxwell model for short times, $t < \tau_M$. Here $G$ is the shear modulus and $p$ a Lagrangian multiplier (effective pressure) ensuring the incompressibility.

Finally, to relate the stretch factor $\lambda$ to its resulting prestress $\sigma_0 = \sigma^0_{xx}$ we can use eq. (2) in the base state prepared by our protocol and get

$$\sigma^0_{xx} = G\left(\lambda^2 - \lambda^{-1}\right) \tag{3}$$

and $\sigma^0_{ij} = 0$ for the other components.

### 2.2 Maxwell model and residual stress

In a nuthsell, the Maxwell model consists of an elastic spring in series with a viscous element. Being in series, both elements experience the same stress and their displacements add. Considering the rate of change of the total displacement, and expressing the two contributions via the stresses, one obtains $\dot{u}_{\mathrm{tot}} = \dot{u}_{\mathrm{elast}} + \dot{u}_{\mathrm{visc}} = \frac{\dot{\sigma}}{G} + \frac{\sigma}{\eta}$, where $G$ is the shear modulus and $\eta$ the shear viscosity. Their ratio defines the characteristic time scale $\tau_M = \eta/G$ of the Maxwell model. At short times, $t < \tau_M$, the behavior is elastic and at long times, $t > \tau_M$, viscous.

The Maxwell model can be generalized to the nonlinear regime by using the symmetric part $\boldsymbol{D} = \frac{1}{2}(\boldsymbol{L} + \boldsymbol{L}^T)$ of

the velocity gradient $\boldsymbol{L} = \frac{\mathrm{d}\boldsymbol{F}}{\mathrm{d}t} \cdot \boldsymbol{F}^{-1} = \nabla \dot{\mathbf{u}}$ for the rate of change of the total displacements, as well as the nonlinear representation of the stress. In the incompressible case and neglecting kinematic nonlinearities [24,25], the respective nonlinear Maxwell model then reads

$$2\boldsymbol{D} = \frac{1}{G}\frac{\partial \tilde{\boldsymbol{\sigma}}}{\partial t} + \frac{\tilde{\boldsymbol{\sigma}}}{\eta}\,. \tag{4}$$

Here, for convenience, we separated the pressure contribution, *i.e.* the Cauchy stress for the Maxwell model is given by $\boldsymbol{\sigma}^{\mathrm{M}} = \tilde{\boldsymbol{\sigma}} - p\boldsymbol{I}$.

We now have prepared a prestressed film, that evolves according to the Maxwell model. However, experimentally it is known that the residual stress relaxes much slower than the instability evolves: above the glass transition temperature, the characteristic time of residual stress relaxation is typically hours [8,19], while the film evolves and becomes unstable within tens of seconds, or minutes [7]. This leads us to propose the following protocol: for $t \leq 0$ the film is deep in the glassy state, $T \ll T_g$, and it behaves as a stressed neo-Hookean solid. For $t \geq 0$ the EHI experiment is started by heating up to $T_{\mathrm{exp}} \gg T_g$. The film liquefies and evolves in the presence of both the residual and electric stresses according to the Maxwell model. Due to the separation of times scales mentioned above, we assume that the residual stress does not vary on the time scale of the instability. We hence can write $\tilde{\boldsymbol{\sigma}} = \tilde{\boldsymbol{\sigma}}_0 + \tilde{\boldsymbol{\sigma}}_1$ and identify $\tilde{\boldsymbol{\sigma}}_0 = G\boldsymbol{B}$. The next order, $\tilde{\boldsymbol{\sigma}}_1$, is determined by the Maxwell model, *i.e.* eq. (4). To summarize, the assumed protocol can be written as

$$t \leq 0 \;:\quad \boldsymbol{\sigma} = \boldsymbol{\sigma}^{\mathrm{NH}} = \tilde{\boldsymbol{\sigma}}_0 - p\boldsymbol{I}\,, \tag{5}$$

$$t \geq 0 \;:\quad \boldsymbol{\sigma} = \tilde{\boldsymbol{\sigma}}_0 + \tilde{\boldsymbol{\sigma}}_1 - p\boldsymbol{I}\,,$$

$$\text{where } 2\boldsymbol{D} = \frac{1}{G}\frac{\partial \tilde{\boldsymbol{\sigma}}_1}{\partial t} + \frac{\tilde{\boldsymbol{\sigma}}_1}{\eta}\,. \tag{6}$$

Note that the use of the Maxwell model guarantees that the transition is continuous. Also note that within the approximation of stationary residual stress, the stress and hence also the stretch factor $\lambda$ enters the dynamics only via the boundary conditions, not in the bulk equations.

Using the Laplace transform ($\tilde{\boldsymbol{\sigma}}_1, \boldsymbol{D} \propto e^{st}$), the equation for $\tilde{\boldsymbol{\sigma}}_1$ can be expressed as

$$\tilde{\boldsymbol{\sigma}}_1 = 2\frac{\eta G}{s\eta + G}\boldsymbol{D} = 2\bar{\eta}\boldsymbol{D} \tag{7}$$

with $\bar{\eta} = \frac{\eta G}{s\eta + G}$ a generalized viscosity.

Finally it remains to specify the force balance, which reads [26]

$$\rho\frac{\partial^2 \mathbf{u}}{\partial t^2} = \boldsymbol{\nabla}\cdot\boldsymbol{\sigma} = \boldsymbol{\nabla}\cdot\left(\tilde{\boldsymbol{\sigma}}_1 - p\boldsymbol{I}\right)\,. \tag{8}$$

Although effects of inertia are very small, cf. below, it is known that total neglect can cause divergences in the growth rates for high electric fields [15]. Hence we keep inertia and briefly discuss when its inclusion is important at the end of sect. 5.

### 2.3 Boundary conditions

*Film-substrate.* In previous works on (visco-)elastic solids [17,18] we considered two different and archetypal boundary conditions (BCs) between the film and the substrate. First, the "fixed BC", $u_x(z = -h_0) = 0$, where the substrate's position is at $z = -h_0$. This BC imposes a vanishing displacement at the substrate —in addition we impose $u_z(z = -h_0) = 0$, *i.e.* the film is not allowed to debond— corresponding to a situation where the polymers and hence the film are strongly adsorbed to the substrate. The second case is the "perfect slip BC", given by $\sigma_{xz}\,(z = -h_0) = 0$. This BC allows for displacements along the substrate, without shear stress, and corresponds to very slippery situations, *e.g.* to films cast on an incompatible polymer brush attached to the substrate, as typically used for dewetting studies [5,10].

In fact, one can treat the general case, which we call "imperfect gliding", by imposing

$$\beta\dot{u}_x\,(z = -h_0) - \sigma_{xz}\,(z = -h_0) = 0\,. \tag{9}$$

This BC can be motivated as follows: The force on the surface is given by $\mathbf{f} = \boldsymbol{\sigma}\,(z = -h_0)\cdot(-\hat{\mathbf{e}}_z)$, where $\hat{\mathbf{e}}_z$ is the unit vector normal to the surface. In presence of friction, the projection of this force along the substrate, $f_x = \hat{\mathbf{e}}_x \cdot \mathbf{f}$ must equal the friction force $-\beta\dot{u}_x\,(x, z = -h_0;\, t)$. This is the so-called Navier condition, where $\beta$ is a friction coefficient [27–29]. Assuming a viscous response in the bulk, one can get access to the friction coefficient via the measurable slip length $\chi = \eta/\beta$ [27].

Note that eq. (9) interpolates between the two above-described limiting cases: perfect gliding is regained in the limit $\beta \to 0$. For $\beta \to \infty$, one gets $\dot{u}_x = 0$ and as initially $u_x = 0$, the fixed BC. In the following we will use the general BC given by eq. (9) and discuss, when instructive, also its limits.

*Free surface.* The general BC for a free surface states that the normal stress $\boldsymbol{\sigma}\cdot\hat{\mathbf{n}}$ (where $\hat{\mathbf{n}}$ is the unit vector normal to the surface) has to match the force $\mathbf{f}_s$ acting on the surface. The free surface is located at $z = 0$ and parameterized by

$$\zeta\,(x,t) = \epsilon h e^{(ikx+st)}\,, \tag{10}$$

where $h$ is the amplitude of a surface perturbation, $k$ its wave number and $s = s(k)$ its associated growth rate. $\epsilon$ is a book-keeping parameter to track orders in $h$. Then the BC at the free surface reads

$$\boldsymbol{\sigma}\,(x, z = \zeta)\cdot\hat{\mathbf{n}} = \mathbf{f}_s\,, \tag{11}$$

where the surface force $\mathbf{f}_s = \mathbf{f}_\gamma + \mathbf{f}_E$ has two contributions, surface tension and electric stress [22]. The surface tension is given by $\mathbf{f}_\gamma \simeq \gamma\left(\partial_x^2\zeta\right)\hat{\mathbf{n}}$, where we kept only the leading order in height perturbation. Assuming a perfect dielectric polymer film, the electric stress results from the Maxwell tensor [30], $T_{ij}^{(\alpha)} = \epsilon_\alpha\epsilon_0\left[E_i^{(\alpha)}E_j^{(\alpha)} - \frac{1}{2}\left(E^{(\alpha)}\right)^2\delta_{ij}\right]$, where $\mathbf{E}$ is the electric field and the indices $\alpha = 1, 2$ denote the polymer film (with $\epsilon_1 > 1$) and the gap (with $\epsilon_2 = 1$ for

air), respectively. As derived earlier [31,17] by solving a classical electrostatics problem, the force due to the electric stresses reads to first order in height perturbation

$$\mathbf{f}_E = (F + Y(k)\zeta)\,\hat{\mathbf{n}}\,, \tag{12}$$

where

$$F = \frac{1}{2}\frac{\epsilon_0\epsilon_1\epsilon_2(\epsilon_1-\epsilon_2)V^2}{(\epsilon_2 h_0 + (d-h_0)\,\epsilon_1)^2}\,, \tag{13}$$

$$Y(k) = \frac{2kF(\epsilon_1-\epsilon_2)}{[\epsilon_1\tanh((d-h_0)\,k) + \epsilon_2\tanh(h_0 k)]}\,. \tag{14}$$

The contribution $F$ is the force acting at the top of a flat surface, while modulations of the surface, $\zeta \neq 0$, give rise to the term $\propto Y(k)$. Note that in contrast to the simpler case of Van der Waals forces acting on the film's surface by approaching a contactor [32,33] (where $Y$ is a constant), electric field lines become curved by surface modulations, inducing the $k$-dependence of $Y(k)$. Also note that both $F$ and $Y$ are strictly positive for $\epsilon_1 > \epsilon_2$.

## 3 Linear stability analysis

Now we can study the growth rates of surface modulations, to determine the dynamics of the instability of the polymer film under the combined action of residual and electric stresses. Details can be found in appendix A.

We consider the plane strain situation, *i.e.* $u_y = 0$ and no $y$-dependence of any variable. The base state is characterized by the homogeneous solution, given by $u_x = 0 = u_z$ and $p_0 = G\lambda^{-1} - F$. Using the ansatz

$$\begin{aligned} u_x(x,z,t) &= \varepsilon\tilde{u}_x(z)\,e^{ikx+st}\,,\\ u_z(x,z,t) &= \varepsilon\tilde{u}_z(z)\,e^{ikx+st}\,,\\ p(x,z,t) &= \tilde{p}_0 + \varepsilon\tilde{p}_1(z)\,e^{ikx+st}\,, \end{aligned}$$

and the incompressibility condition, $\partial_x\tilde{u}_x + \partial_z\tilde{u}_z = 0$, yields a single equation for $\tilde{u}_z$,

$$l^2k^2\tilde{u}_z - \left(k^2+l^2\right)\tilde{u}_z^{(2)} + \tilde{u}_z^{(4)} = 0\,. \tag{15}$$

Here the superscript $(n)$ means the $n$-th derivative with respect to $z$ and

$$l = \sqrt{k^2 + \frac{s\rho}{\bar{\eta}}} = \sqrt{k^2 + \frac{s\rho(s\eta+G)}{\eta G}} \tag{16}$$

is an inverse length scale that depends both on the elastic properties (shear modulus) and the dynamic properties (viscosity, inertia, as well as the time scale of the perturbation).

The general solution of eq. (15) reads [34]

$$\begin{aligned} \tilde{u}_z = {} & A_1\cosh\left[k\,(z+h_0)\right] + A_2\cosh\left[l\,(z+h_0)\right]\\ & + B_1\sinh\left[k\,(z+h_0)\right] + B_2\sinh\left[l\,(z+h_0)\right]\,. \end{aligned} \tag{17}$$

The coefficients $A_1$, $A_2$, $B_1$ and $B_2$, functions of $k$ and $s$, have to be obtained by imposing the BCs at the substrate, eq. (9), and for the free surface, eq. (11). Since one has to account for the full stress, $\tilde{\boldsymbol{\sigma}} = \tilde{\boldsymbol{\sigma}}_0 + \tilde{\boldsymbol{\sigma}}_1$, note that the stretch parameter describing the residual stress enters the coefficients.

Finally, the condition to have nontrivial, *i.e.* spatially modulated, solutions is obtained by imposing that the vertical displacement at the free surface has to match the undulation perturbation: $\tilde{u}_z(z=0) = h$, cf. the definition of $\zeta$ in eq. (10). This leads to an equation of the form

$$hZ(k,s) = 0\,, \tag{18}$$

where [35]

$$\begin{aligned} Z(k,s) = {} & \big[A_1\cosh(kh_0) + A_2\cosh(lh_0) +\\ & + B_1\sinh(kh_0) + B_2\sinh(lh_0)\big]/h - 1\,. \end{aligned} \tag{19}$$

Any pair $(k^*, s(k^*))$ of a real $k^*$ with a, in general complex, $s(k^*)$ that fulfills $Z(k^*, s(k^*)) = 0$ corresponds to an undulation of the surface with wave number $k^*$ and growth rate $s(k^*)$. Except for simple limiting cases, the growth rates have to be obtained numerically. Before discussing the results, we briefly overview the important parameters.

## 4 Parameters

It is suitable to rescale the problem by introducing dimensionless units. We scale time in units of the Maxwell time and space in units of the film thickness, by writing

$$S = \tau_M s = \frac{\eta}{G}s\,, \quad K = h_0 k\,, \quad L = h_0 l\,. \tag{20}$$

There are five remaining dimensionless parameters determining the behavior of the system: first of all the stretch factor $\lambda$. Further on the electric stress and the surface tension, both rescaled by film thickness and shear modulus, yielding $Y = \frac{h_0}{G}Y(K)$ and $\Gamma = \frac{\gamma}{Gh_0}$, respectively. The rescaled BC parameter $b = \frac{\beta h_0}{\eta} = \frac{h_0}{\chi}$ has still the limiting cases $b = 0$ corresponding to the perfect slip BC and $b \to \infty$ to the fixed BC. Finally $R = \frac{\rho G h_0^2}{\eta^2}$ determines the importance of inertia.

In the following we use parameters typical for the experimental system studied in ref. [7]: film thickness $h_0 = 100\,\mathrm{nm}$; distance between the capacitor plates $d = 4h_0$, which could be experimentally achieved by using colloidal spacers; polystyrene (PS) elastic modulus $G \simeq 6\cdot10^5\,\mathrm{Pa}$; PS viscosity $\eta \simeq 2.2\cdot10^3\,\mathrm{Pa\,s}$, corresponding to a molecular weight of $\simeq$ 30–50 kg/mol; PS surface tension $\gamma \simeq 30\,\mathrm{mN/m}$; PS density $\rho \simeq 10^3\,\mathrm{kg/m^3}$; dielectric constants $\epsilon_1 = 2.5$ (PS), $\epsilon_2 = 1$ (air); typical experimental voltages are $V = 5$–$100\,\mathrm{V}$, we use also higher values; finally, the friction coefficient can be estimated to be $\beta \approx 2\cdot10^{10}\,\mathrm{kg\,m^{-2}\,s^{-3}}$ for the given viscosity and a typical slip length of $\chi \simeq 100\,\mathrm{nm}$ [36]. With these parameters, we get $\tau_M = \frac{\eta}{G} = 0.036\,\mathrm{s}$, as well as the following dimensionless quantities: $\Gamma \simeq 0.5$, $b \simeq 1$, $R \simeq 1.2\cdot10^{-14}$.

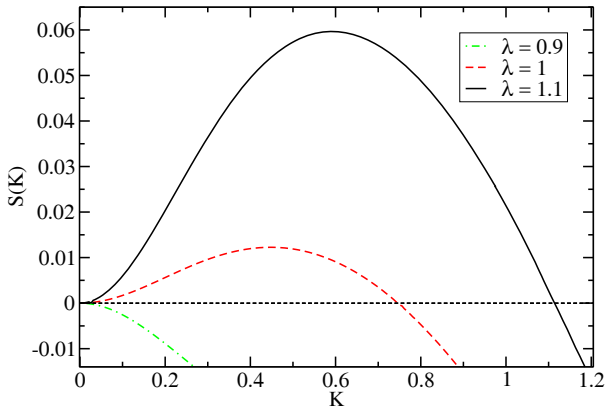


**Fig. 1.** (Color online) The renormalized growth rate $S(K)$ as a function of the renormalized wave number $K$ for an electric stress corresponding to 100 V and for stretch factors $\lambda = 0.9$ (corresponding compressive stress $\sigma_0 = -54$ kPa; dash-dotted), $\lambda = 1$ (no residual stress; dashed) and $\lambda = 1.1$ (corresponding tensile stress $\sigma_0 = 66$ kPa; solid). Parameters: $b = 1$, $\Gamma = 0.5$, $R = 1.2 \cdot 10^{-14}$.

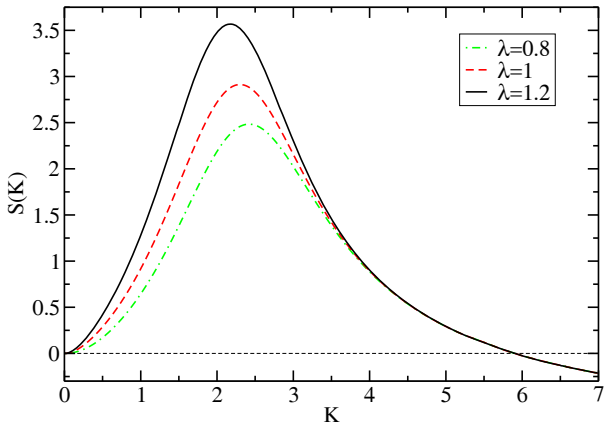


**Fig. 2.** (Color online) The renormalized growth rate $S(K)$ as a function of the renormalized wave number $K$ for an electric stress corresponding to 300 V and for stretch factors $\lambda = 0.8$ (compressive stress $\sigma_0 = -96$ kPa; dash-dotted), $\lambda = 1$ (no stress; dashed) and $\lambda = 1.2$ (tensile stress $\sigma_0 = 144$ kPa; solid). Other parameters as in fig. 1.

## 5 Results and discussions

The main question that arises is how the two stresses —the in-plane elastic residual stress stemming from the spin-coating process, and the normal electric stress induced by the application of the external electric field— interplay in the destabilization of the film. Our main focus will lie on the behavior of the fastest growing wave number, which dominates the initial growth. In addition, it should be noted that due to the proximity of the two capacitor plates (with the distance of the order of the film's thickness), the fastest-growing wave number will also roughly determine the final experimentally achieved pattern, consisting of columns of polymer material bridging the capacitor plates.

Figure 1 shows the renormalized growth rate $S(K)$ as a function of the renormalized wave number $K$ for an electric stress corresponding to 100 V and stretch factors in the range $\lambda = 0.9$–$1.1$ corresponding to stresses as specified in the figure caption. Note that modes (of surface perturbations) with positive growth rate, $S(K) > 0$, will grow while those with negative growth rates are damped. One can see that for the given voltage, the stability is very sensitive to the frozen-in residual stress: already a moderate compressive stress completely stabilizes the system while a tensile stress increases [37] the maximum growth rate substantially, about five-fold. A higher fastest growth rate (as exemplified for the tensile stress compared to the case in the absence of stress) is concomitant with a larger fastest growing wave number, $K_{\rm fg}$, *i.e.* the maximum of the growth rate determined by $\frac{\partial S}{\partial K}|_{K_{\rm fg}} = 0$.

But the situation is more complex: Figure 2 shows a similar plot for a higher electric stress corresponding to 300 V. Still the system under tension is more unstable then the unstressed or compressed cases. However, now the higher fastest growth rate is associated to a smaller wave number, *i.e.* a *larger* wavelength. This behavior may explain the recent puzzle concerning the experimentally observed wavelengths by Barbero *et al.* [7]: there the wavelengths were systematically larger for freshly spin-cast (stressed) films than for old (unstressed) films. This seemed to be counterintuitive, since a system with several destabilizing factors should be more unstable and display a smaller wavelength. The situation shown in fig. 2 is in qualitative accordance: fresh films, in our interpretation corresponding to a high in-plane tensile stress, *i.e.* $\lambda > 1$, can display an instability with a larger wavelength than old films, corresponding to $\lambda \simeq 1$. So although maybe counterintuitive, in a nonlinear situation there is no special reason why two destabilizing stresses —and even more so if they act in different directions— should simply add.

To investigate this behavior in more detail, fig. 3 shows the dependence of the fastest growing wave number $K_{\rm fg}$ as a function of the residual stress and for different voltages. In the upper panel, the black curve corresponds to fig. 1 and shows how $K_{\rm fg}$ grows with increasing $\lambda$. The blue curve corresponds to fig. 2 displaying the opposite trend. In between there is a voltage ($\simeq 150$ V for the given parameters; shown in red) where there is basically no dependence of $K_{\rm fg}$ on the residual stress (albeit still the growth rate will depend on it). Note that all curves end at a lower bound for $\lambda$, where the compressive stress stabilizes the system, cf. fig. 1, and where $K_{\rm fg}$ ceases to exist. The lower panel of fig. 3 shows the influence of the viscoelastic properties: a ten-fold increase in the viscosity shifts the change in slope to lower voltages, and in addition the negative slope for high voltages becomes more pronounced. Note that it is not only the Maxwell time $\tau_M = \eta/G$ that determines the behavior: a ten-fold increase in viscosity and a ten-fold decrease in shear modulus lead to different results, since shear modulus and viscosity enter the problem in different ways.

Figures 1 to 3 have been obtained by numerically solving eq. (18), but some analytical insight can also be

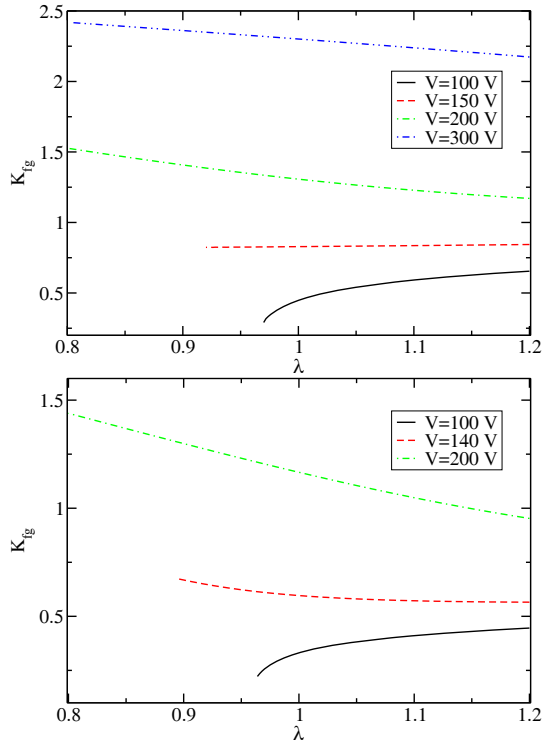


**Fig. 3.** (Color online) Shown is the dependence of the renormalized fastest growing wave number, $K_{\rm fg}$, as a function of the stretch factor $\lambda$ for different applied voltages as indicated in the legend. Upper panel: the overall behavior changes at $\simeq 150\,\mathrm{V}$ from $K_{\rm fg}$ increasing with $\lambda$ for lower voltages to $K_{\rm fg}$ decreasing with $\lambda$ for higher voltages. Lower panel: the same plot, but with the viscosity increased ten-fold (corresponding to $\eta = 2.2 \cdot 10^4\,\mathrm{Pa\,s}$). The change in behavior is shifted towards lower voltages and the negative slopes at high voltages are more pronounced. Other parameters as in fig. 1.

obtained. First of all, note that $S(K=0)$ is always zero. This simply reflects the fact that the zero wave number mode, corresponding to a homogeneous movement of the surface, is prohibited by incompressibility. Hence as soon as the curvature of the growth rate at $K=0$ is positive, $\frac{\partial^2 S}{\partial K^2}_{|K=0} > 0$, the film gets unstable. For not too small $b$ (note the divergence for $b \to 0$ of eq. (21) and cf. the discussion of fig. 5 below) it is given by

$$\frac{\partial^2 S}{\partial K^2}_{|K=0} = \frac{2(3+b)\lambda Y_0 + 3(2+b)(\lambda^3-1)}{6b\lambda}\,, \qquad (21)$$

where $Y_0 = Y(K{=}0)$. Expanding for small stresses, $\lambda = 1+\delta$ with $|\delta| \ll 1$, leads to

$$\frac{\partial^2 S}{\partial K^2}_{|K=0} \simeq \frac{(3+b)Y_0}{3b} + \frac{3(2+b)}{2b}\delta + \frac{2+b}{2b}\delta^3 + \ldots\,. \qquad (22)$$

One clearly sees that, first, the electric field is always destabilizing since $Y_0 > 0$. Second, in accordance with figs. 1 and 2, a tensile stress ($\delta > 0$) destabilizes, while a compression ($\delta < 0$) stabilizes.

In a rather small parameter range, the case occurs where small wave numbers are stabilized by compressive

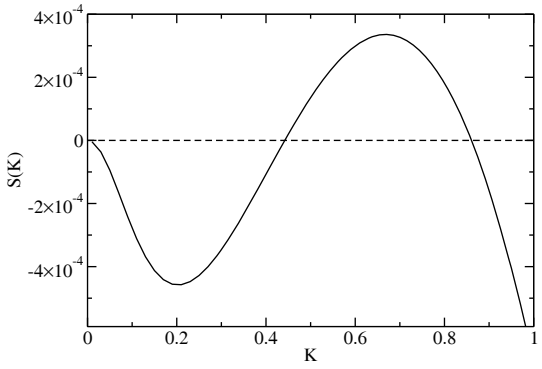


**Fig. 4.** (Color online) The renormalized growth rate $S(K)$ as a function of the renormalized wave number, showing the case where compressive stress stabilizes small wave numbers but where, due to the combined action of electric field and viscoelasticity, a finite window of unstable wave numbers exists. Parameters: $\lambda = 0.9$, $V = 140\,\mathrm{V}$, $\eta = 2.2 \cdot 10^4\,\mathrm{Pa\,s}$ implying $b = 0.1$, others as in fig. 1.

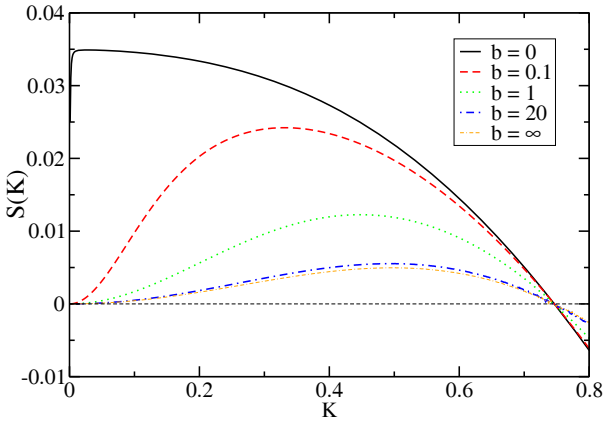


**Fig. 5.** (Color online) The renormalized growth rate $S(K)$ as a function of the renormalized wave number $K$ for varying parameter $b$ (renormalized friction at the substrate; $b = 0$ perfect slip, $b \to \infty$ perfectly sticking). The applied electric stress corresponds to 100 V, the in-plane stress is zero ($\lambda = 1$; the behavior is similar for finite stretch factors). Other parameters as in fig. 1.

stress while finite wave numbers are unstable: as shown in fig. 4, the curvature $\frac{\partial^2 S}{\partial K^2}_{|K=0}$ at $K=0$ is negative, but due to the combined effect of electric destabilization and viscoelasticity [38], $S(K)$ increases again to yield a finite window of wave numbers with positive growth rate. This case may be interesting, since such a type of instability is known to lead to persistent patterns with a finite, well-defined wavelength [39] —as the system is not able to coarsen since long wavelengths cannot grow.

To study the effect of the boundary condition at the substrate, fig. 5 displays the renormalized growth rate $S(K)$ for a voltage of 100 V and for varying parameter $b$. We represented the case in the absence of stress (in the presence of stress the behavior is similar; the green curve corresponds to the red curve of fig. 1). First one can notice that the largest unstable wave number $K_{\rm max}$ (defined

by $S(K_{\max}) = 0$, and separating the unstable range with $S(K) > 0$ for $K < K_{\max}$ from $S(K) < 0$ for $K > K_{\max}$) is almost not sensitive to the boundary condition used (it is strictly not sensitive in the case $\lambda = 1$). However, the fastest growing wave number $K_{\rm fg}$ —which determines the initial growth and often also the experimentally obtained pattern for small capacitor gaps— is very sensitive: for intermediate values of $b$, $K_{\rm fg}$ decreases with $b$. For $b \simeq 20$ and larger, there is no noticeable change anymore and the film behaves as sticking perfectly to the substrate.

The limit $b \to 0$ is subtle. Inspecting eq. (21), the curvature at $K = 0$ is always positive, becomes very steep (cf. the black solid curve in fig. 5) and finally diverges for $b \to 0$. Performing $b \to 0$ and $R \to 0$ yields a growth rate that has $S(K{=}0) = 0$ —as forced by incompressibility— but then jumps to a finite value $S(K \searrow 0) = S(0^+) \neq 0$ with *negative* curvature. As a cross check, the same result is obtained by applying the "perfect slip BC" directly from the start. Analytically, one gets

$$S(0^+) = \frac{\lambda^3 - 1 + \lambda Y_0}{1 - \lambda^3 + \lambda(4 - Y_0)}\,, \qquad (23)$$

which corresponds well to an extrapolation for very low values of $b$, cf. the solid black curve in fig. 5.

Concluding the dependence on the boundary conditions, the imperfect gliding condition, eq. (9), indeed interpolates between gliding perfectly along the substrate and being rigidly fixed to the substrate. The fastest growing wave number is very sensitive to the boundary condition at the substrate, varying from a finite value —of the order of $K_{\max}$— for large $b$ to almost zero (corresponding in a finite system to the largest possible wavelength) for small $b$. The influence is quite dramatic for $b < 1$, *i.e.* for strong slippage.

The behavior of $K_{\rm fg}$ —cf. figs. 3 and 5— as a function of parameters is not accessible analytically. However, the dependence of the maximum unstable wave number $K_{\max}$ around $\lambda = 1$ can be discussed. When $\lambda = 1$, $K_{\max}$ is given by the solution of $Y(K_0)/K_0^2 = \Gamma$. In the general case $\lambda \neq 0$, one has to solve

$$\frac{Y(K)}{K^2} = \Gamma + \frac{2(2+b)(\lambda^3 - 1)/\lambda}{2K[1 + b - \cosh(2K)] - b\sinh(2K)}\,. \qquad (24)$$

For $\lambda = 1 + \delta$ with $|\delta| \ll 1$, to leading order one gets $K_{\max} = K_0 + \delta K_1$ with

$$K_1 = \frac{6(2+b)K_0^2\left(2K_0\Gamma + (\partial_K Y)_{|K=K_0}\right)^{-1}}{2K_0\left[1 + b - \cosh(2K_0)\right] - b\sinh(2K_0)}\,. \qquad (25)$$

It is easy to verify that $K_1 > 0$ (note that $\partial_K Y > 0$), meaning that a small stretch increases $K_{\max}$, while a small compression decreases it. For $\lambda = 1$, $K_{\max}$ is independent of the boundary condition used, cf. also fig. 5. For finite stress, the correction has a (small) dependence on $b$.

Finally, let us briefly discuss the effect of inertia, *i.e.* why respectively when it is necessary to use eq. (8) instead of the static force balance $\nabla\cdot\boldsymbol{\sigma} = 0$. This is a known issue,

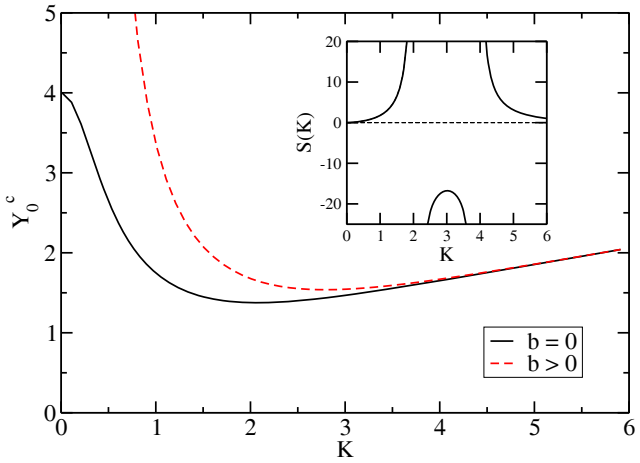


**Fig. 6.** (Color online) Shown is the value $Y_0^c$ for the electric stress for which a divergence in the growth rate $S(K)$ occurs if inertia is neglected (*i.e.* for $R = 0$; a typical diverging growth rate is shown in the inset, corresponding to $b > 0$ and $V = 350\,\mathrm{V}$). The solid curve corresponds to $b = 0$ (perfect slip), while the dashed curve is for $b > 0$ (imperfect gliding, or sticking). In-plane stress was neglected, $\lambda = 1$.

and was discussed in detail in ref. [15] for a leaky dielectric film (instead of a perfect dielectric as discussed here) and in the absence of stress: namely, for high destabilization —high voltage, and high tensile stress— the implicit solution $S(K)$ of eq. (18) displays divergences for certain wave numbers, cf. the inset of fig. 6. It was shown in ref. [15] that any finite value of inertia ($R \neq 0$) removes these divergences, restoring the generic form of the growth rates, as shown in *e.g.* fig. 2. For the given parameters, we have $R = 1.2 \cdot 10^{-14}$ which is indeed very small, but however not negligible at high destabilization.

Figure 6 displays the value $Y_0^c$ of the electric stress where such divergences in the growth rate start to manifest themselves if inertia is neglected, *i.e.* for $R = 0$. The solid curve corresponds to $b = 0$ (perfect slip) and was obtained by performing the limit $R \to 0$, and then $b \to 0$. The dashed curve is for finite $b$ (imperfect gliding, including sticking). In-plane stress was neglected, $\lambda = 1$, but the behavior is similar under stress. The minimum at finite wave numbers cannot be obtained analytically, but one can get an estimate by looking at $K = 0$ in case of $b = 0$, where the denominator in eq. (23) yields the divergence condition leading to $Y^c(K{=}0) = 4 - \frac{\lambda^3 - 1}{\lambda}$. This coincides with the value for $K = 0$ of the solid black curve in fig. 6 and also shows that finite stresses yield only a small correction (since $3\delta \ll 4$ if $\lambda = 1 + \delta$). From the figure one can see that for the given parameters, inertia effects can be neglected for $Y_0$ below $\approx 1.54$ (corresponding voltage $V \simeq 337\,\mathrm{V}$; in case $b > 0$), and $\approx 1.38$ (corresponding voltage $V \simeq 319\,\mathrm{V}$, in case $b = 0$), respectively.

We can conclude that for typical voltages used in EHI for polymer films, inertia can be safely neglected, except if the shear modulus is much smaller than the one taken in this study.

## 6 Conclusions

We studied the response of a viscoelastic thin polymer film to an in-plane internal residual stress and an externally applied electric stress normal to the surface. First, the tensile residual stress accelerates the instability, *i.e.* leads to faster growth rates of the surface undulations. Second, for high enough voltages, the characteristic wavelength of the instability can be larger in the presence of tensile stress then in the unstressed case. Both results are in qualitative agreement with experiments studying the electro-hydrodynamic instability of freshly spin-cast (*i.e.* stressed) *vs.* aged films (*i.e.* un- or less stressed) of high molecular weight polystyrene [7]. A direct comparison is difficult as the Maxwell model —having a single relaxation time— is too simple to describe the constitutive behavior of a real polymer film. Nevertheless the trend for the wavelength (increasing wavelength for increasing destabilization) obtained in the Maxwell model hints at the possibility that this puzzling behavior may be explained without invoking additional complex properties (like inhomogeneities, variations in the entanglement density or a polymer crust due to evaporation, etc.).

The theoretical results should also be compared to the case of a purely elastic film (allowing for surface diffusion of polymers) studied in ref. [17]. We will not do this in all detail here, but however would like to highlight the following generic features: in the elastic system, the in-plane stress destabilizes the system via the well-known Asaro-Tiller-Grinfeld (ATG) mechanism [40,41]. The addition of the electric stress breaks the symmetry of the ATG instability —compressive and tensile stresses destabilize differently, in contrast to ATG in the absence of electric field. In the viscoelastic (Maxwell) fluid case, a compressive stress stabilizes and a tensile stress —as is the case in spin-cast films— destabilizes the film, independent of the applied voltage. Interestingly, the addition of the electric stress still has a non-trivial effect, namely the change in the behavior of the wavelength of the fastest growing mode (as discussed already above) with the applied voltage.

## Appendix A.

The general solution of eq. (15) reads

$$u_z = A_1 \cosh\left[k\,(z+h_0)\right] + A_2 \cosh\left[l\,(z+h_0)\right] + B_1 \sinh\left[k\,(z+h_0)\right] + B_2 \sinh\left[l\,(z+h_0)\right]. \quad \text{(A.1)}$$

The boundary conditions between the film and the substrate read

$$u_z(z=-h_0)=0 \iff A_2=-A_1\,, \quad \text{(A.2)}$$

$$\sigma_{xz}(z=-h_0)=s\beta u_x(z=-h_0) \iff A_2=-\beta\frac{kB_1+lB_2}{\bar\eta(k^2-l^2)}\,, \quad \text{(A.3)}$$

where (A.3) has been Laplace transformed. The boundary conditions at the free surface read, in first order of the height perturbation

$$\epsilon\tilde\sigma_{1,zz}-\epsilon\tilde p_1=(Y(k)-\gamma k^2)\zeta\,, \quad \text{(A.4)}$$

$$\epsilon\tilde\sigma_{1,xz}+ik\zeta G(\lambda^2-\lambda^{-1})=0\,. \quad \text{(A.5)}$$

Note that the $\lambda$-dependence in eq. (A.5) stems from $\tilde\sigma_0$. These equations determine

$$B_1=\frac{2hk\rho}{\bar\eta^2\lambda(k^2-l^2)}\frac{\bar\eta(k^2-l^2)N_{11}+\beta N_{12}}{\bar\eta(k^2-l^2)D_1+\beta D_2}\,, \quad \text{(A.6)}$$

$$B_2=-\frac{2hk^2\rho}{\bar\eta^2\lambda(k^2-l^2)}\frac{\bar\eta(k^2-l^2)N_{21}+\beta N_{22}}{\bar\eta(k^2-l^2)D_1+\beta D_2}\,, \quad \text{(A.7)}$$

where

$$\begin{aligned}
N_{11} &= 2Gk^2l(\lambda^3-1)\cosh\left[lh_0\right] \\
&\quad -(k^2+l^2)\lambda(Y-k^2\gamma)\sinh\left[lh_0\right], \\
N_{12} &= lN_{22}, \\
N_{21} &= G(k^2+l^2)(\lambda^3-1)\cosh\left[kh_0\right] \\
&\quad -2k\lambda(Y-k^2\gamma)\sinh\left[kh_0\right], \\
N_{22} &= \lambda(Y-k^2\gamma)\left((k^2+l^2)\cosh\left[lh_0\right]-2k^2\cosh\left[kh_0\right]\right) \\
&\quad +Gk(\lambda^3-1)\left((k^2+l^2)\sinh\left[kh_0\right]-2kl\sinh\left[lh_0\right]\right), \\
D_1 &= (l^4+2l^2k^2+4lk^3+k^4)\sinh\left[(k-l)h_0\right] \\
&\quad +(l^4+2l^2k^2-4lk^3+k^4)\sinh\left[(k+l)h_0\right], \\
D_2 &= 8k^2l(k^2+l^2)+(k-l)^2(-l^3-3lk^2 \\
&\quad -l^2k+k^3)\cosh\left[(k+l)h_0\right] \\
&\quad -(k+l)^2(l^3+3lk^2-l^2k+k^3)\cosh\left[(k-l)h_0\right].
\end{aligned}$$

Note that the same coefficients $A_1$, $A_2$, $B_1$, $B_2$ determine also $Z(k)$, cf. eq. (19), which determines the growth rate $s(k)$ via eq. (18).

## References


1. G. Reiter, Adv. Polym. Sci. **252**, 29 (2013).
2. R. Blossey, *Thin Liquid Films: Dewetting and Polymer Flow* (Springer, Dordrecht, 2012).
3. S.G. Croll, J. Appl. Polym. Sci. **23**, 847 (1979).
4. K. Norrman, A. Ghanbari-Siahkali, N.B. Larsen, Annu. Rep. Prog. Chem., Sect. C **101**, 174 (2005).
5. G. Reiter, M. Hamieh, P. Damman, S. Sclavons, S. Gabriele, T. Vilmin, E. Raphaël, Nat. Mater. **4**, 754 (2005).
6. H. Bodiguel, C. Fretigny, Eur. Phys. J. E **19**, 185 (2006).
7. D.R. Barbero, U. Steiner, Phys. Rev. Lett. **102**, 248303 (2009).
8. J.Y. Chung, T.Q. Chastek, M.J. Fasolka, H.W. Ro, C.M. Stafford, ACS Nano **3**, 844 (2009).
9. K. Thomas, U. Steiner, Soft Matter **7**, 7839 (2011).
10. M. Chowdhury, P. Freyberg, F. Ziebert, A.C.M. Yang, U. Steiner, G. Reiter, Phys. Rev. Lett. **109**, 136102 (2012).

11. T. Vilmin, E. Raphaël, Eur. Phys. J. E **21**, 161 (2006).
12. F. Ziebert, E. Raphaël, Phys. Rev. E **79**, 031605 (2009).
13. E. Schäffer, T. Thurn-Albrecht, T.P. Russell, U. Steiner, Europhys. Lett. **53**, 518 (2001).
14. J. Sarkar, A. Sharma, V. Shenoy, Phys. Rev. E **77**, 031604 (2008).
15. G. Tomar, V. Shankar, A. Sharma, G. Biswas, J. Non-Newtonian Fluid Mech. **143**, 120 (2007).
16. L.F. Pease III, W.B. Russel, J. Non-Newtonian Fluid Mech. **102**, 233 (2002).
17. F. Closa, F. Ziebert, E. Raphaël, Phys. Rev. E **83**, 051603 (2011).
18. F. Closa, F. Ziebert, E. Raphaël, Math. Model. Nat. Phenom. **7**, 6 (2012).
19. K. Thomas, A. Chenneviere, G. Reiter, U. Steiner, Phys. Rev. E **83**, 021804 (2011).
20. The small conductivity of a polystyrene melt, $\sigma \propto 10^{-18}\,\Omega^{-1}\mathrm{m}^{-1}$ leads to characteristic times for the displacement of charges of around $\epsilon/\sigma \propto 10^6$ s where $\epsilon \simeq 2.5\epsilon_0$ is the permittivity. Hence charge displacements can be neglected during the growth of the instability.
21. J.R. Melcher, G.I. Taylor, Annu. Rev. Fluid Mech. **1**, 111 (1969).
22. Y. Tsori, Rev. Mod. Phys. **81**, 1471 (2009).
23. C.W. Macosko, *Rheology: Principles, Measurements, and Applications* (Wiley, New York, 1994).
24. To first order in height perturbation, the convective nonlinearities do not play a role.
25. G. Tomar, V. Shankar, S.K. Shukla, A. Sharma, G. Biswas, Eur. Phys. J. E **20**, 185 (2006).
26. L.D. Landau, E.M. Lifshitz, *Theory of Elasticity* (Pergamon Press, New York, 1986).
27. P.G. de Gennes, Langmuir **18**, 3413 (2002).
28. M. Behr, Int. J. Num. Meth. Fluids **45**, 43 (2004).
29. X.H. Pan, S.Q. Huang, S.W. Yu, X.Q. Feng, J. Phys. D: Appl. Phys. **42**, 055302 (2009).
30. J.D. Jackson, *Classical Electrodynamics* (Wiley, New York, 1998).
31. A. Onuki, Physica A **217**, 38 (1995).
32. A. Ghatak, M.K. Chaudhury, V. Shenoy, A. Sharma, Phys. Rev. Lett. **85**, 4329 (2000).
33. V. Shenoy, A. Sharma, J. Mech. Phys. Solids **50**, 1155 (2002).
34. Note that in case of $\rho = 0$, *i.e.* without inertia, $l = k$ and the solution of eq. (15) reads

$$\begin{aligned}\tilde{u}_z = {} & A_1 \cosh\left[k\left(z+h_0\right)\right] + A_2\left(z+h_0\right)\cosh\left[k\left(z+h_0\right)\right] \\ & + B_1 \sinh\left[k\left(z+h_0\right)\right] + B_2\left(z+h_0\right)\sinh\left[k\left(z+h_0\right)\right].\end{aligned}$$

35. Note that all coefficients are $\propto h$, hence $Z(k,s)$ does not depend on $h$.
36. R. Fetzer, M. Rauscher, A. Münch, B.A. Wagner, K. Jacobs, Europhys. Lett. **75**, 638 (2006).
37. Note that the opposite behavior concerning tension *vs.* compression has been found for a viscoelastic solid (Voigt-Kelvin model) in [18].
38. This effect is related to viscoelasticity, as it was absent in the purely elastic case studied in [17].
39. M.C. Cross, P.C. Hohenberg, Rev. Mod. Phys. **65**, 851 (1993).
40. M. Grinfeld, Sov. Phys. Dokl. **31**, 831 (1986).
41. R. Asaro, W. Tiller, Metall. Trans. A **3**, 1789 (1972).